

Efficient, fast and principled mean-field inference for strongly coupled data

Hugo Jacquin¹ and A. Rançon²

¹*Laboratoire de Physique Statistique, École Normale Supérieure,
24 rue Lhomond, Paris, France*

²*Laboratoire de Physique, École Normale Supérieure de Lyon,
46 Allée d'Italie, Lyon, France*

We present a new method for inferring pairwise interactions from the correlations of datasets of units that can assume any number of states. Thanks to a principled and systematic approach, our method solves several well known issues of naive mean-field and its more recent refinements. The obtained inference is stable and quantitative even deep in the glassy phase of random spin systems, where other methods fail. Effective fields and couplings are inferred with the correct magnitude by the algorithm, and correlate well with the true couplings and fields used to generate the data, even for large couplings. These can then be used to generate new configurations that have high probability in the original model. Because most of the approach is analytical, the computing cost is very low. We test our approach on the Sherrington-Kirkpatrick model in presence of magnetic fields, and show that it performs very well in the glassy phase, even for small or biased sampling. This is because our approach is self-regularized, an important feature which avoids both resorting to pseudocounts or regularization, as well as over-fitting. Our principled approach can be generalized for applications to various kinds of systems such as restricted Boltzmann machines, inference of continuous signals or temporal data, and biological or neuronal data.

Introduction- Learning putative probability distributions from the sole knowledge of a given sample, or data set, has become an unavoidable task in the field of data science, where one is faced with very large amounts of data, with little or no knowledge of the underlying microscopic model from which these data are derived. Applications can be found in neuroscience [1–3], protein science [4–6], in the study of bird flocks [7] or finance [8]. In all cases, the considered data sets are comprised of M independent measurements of the state of N variables: $(\sigma_1^{(\tau)}, \dots, \sigma_N^{(\tau)})$, with $\tau = 1 \dots M$ and $\sigma_i^{(\tau)} = \pm 1$. Variables with more states (i.e. Potts variables) are treated in the same way but we restrict ourselves to Ising variables for clarity and refer the reader to the supplemental materials for the Potts case. In large data sets, dealing with all the data can be too time-consuming and simple observables like the mean of the elementary units $f_i^M = \frac{1}{M} \sum_{\tau=1}^M \sigma_i^{(\tau)}$ or their pairwise correlations, $p_{ij}^M = \frac{1}{M} \sum_{\tau=1}^M \sigma_i^{(\tau)} \sigma_j^{(\tau)}$ can already be a complex enough description of the data. Starting from this reduced description of the dataset, the least constrained probability reproducing \mathbf{f}^M and \mathbf{p}^M is obtained by the maximum entropy principle [9], which leads to the task of inferring the fields \mathbf{h} and couplings \mathbf{J} of an Ising model (for binary variables) or a Potts model (for variables that can take $q > 2$ states). The model is entirely specified by its partition function $Z[\mathbf{h}, \mathbf{J}] = \sum_{\{\sigma\}} \exp\left(\sum_i h_i \sigma_i + \sum_{i<j} J_{ij} \sigma_i \sigma_j\right)$, and \mathbf{h} and \mathbf{J} must be adjusted so that the model has the one- and two-point marginals \mathbf{f}^M and \mathbf{p}^M .

Technically speaking, the sought for fields and couplings \mathbf{h}^* and \mathbf{J}^* are given by the double Legendre trans-

form of the partition function with respect to \mathbf{h} and \mathbf{J} ,

$$\begin{aligned} \mathcal{S}[\mathbf{f}, \mathbf{p}] &= \ln Z[\mathbf{h}^*, \mathbf{J}^*] - \sum_i h_i^* f_i - \sum_{i<j} J_{ij}^* p_{ij}, \\ \mathbf{h}^*[\mathbf{f}, \mathbf{p}] &\text{ such that } \partial_{h_i} \ln Z[\mathbf{h}^*, \mathbf{J}^*] = f_i, \\ \mathbf{J}^*[\mathbf{f}, \mathbf{p}] &\text{ such that } \partial_{J_{ij}} \ln Z[\mathbf{h}^*, \mathbf{J}^*] = p_{ij}, \end{aligned} \quad (1)$$

and the derivatives of \mathcal{S} with respect to \mathbf{f} and \mathbf{p} give \mathbf{h}^* and \mathbf{J}^* , after evaluation at $\mathbf{f} = \mathbf{f}^M$ and $\mathbf{p} = \mathbf{p}^M$. In addition, $\mathcal{S}[\mathbf{f}^M, \mathbf{p}^M]$ gives an estimate of the Kullback-Leibler divergence between the empirical distribution and the inferred Boltzmann distribution [10].

Because a direct method to numerically optimize Eq. (1) reaches unreasonable computation times already for $N \simeq 20$ [11], one has to find approximate solutions to both compute \mathcal{S} and then minimize it. Many studies have been devoted to this task, and we (artificially) classify them in two classes. A first class of methods, represented by pseudo-likelihood approaches [12, 13] and the adaptive cluster expansion (ACE) [10, 14], first choose an approximation for $\ln Z$, then solve the optimization problem in Eq.(1) by gradient descent or other numerical optimization methods, see also [15–17]. But whenever the considered units interact strongly and densely, and/or M is too large, their computation time explodes, and one has to turn to the second class of (mostly analytical) methods: approaches based on Naive Mean-Field (NMF) and high-temperature expansions [5, 18–20], and approaches based on the Bethe approximation, possibly solved by message-passing algorithms [21–25]. Unfortunately, these analytical methods are generically unable to infer correctly inside a glass phase, or when correlations are strong, see for example [20, 23]. Only NMF can be used in all situations, but has severe drawbacks. Most importantly, the fields inferred by NMF are very wrong as

soon as the data leave the high-temperature regime. Second, NMF implies the inversion of the correlation matrix \mathbf{c}^M of the data (where $c_{ij}^M = p_{ij}^M - f_i^M f_j^M$), that can have zero modes when sampling is not good enough (especially in the glass phase). This last point forces practitioners of NMF-inspired methods to modify the data by including strong pseudocounts [26], or to regularize the inference, which destroys the advantage of having an analytical approximation, since one has then to resort to a numerical optimization over the inference parameters. Attempts to go beyond these fundamental limitations are for the moment scarce, see for example [27, 28]. Although the presence of an underlying glass transition seems to be a hindrance to the success of the inference, it has been argued in [10] that this should not be a limitation. The intuitive argument is that since the inverse problem is characterized by the inverse susceptibility (i.e. how fields and couplings are affected by a change in magnetizations and correlations), the inference should not be hindered by the divergence of the susceptibility due to the glass transition. Of course probing deep inside an ordered phase or a glass phase will lead to data that are very polarized, resulting in bad statistical estimation of correlations, but this problem also affects data that have very small correlations, and is not tantamount of an underlying phase transition. Indeed, numerical methods like the ACE or pseudo-likelihood are not affected by the glass transition [13, 14].

Resummed mean-field approximation- In this paper we present a novel mean-field inference method -the resummed mean-field approximation (RMF)- that solves the issues of NMF, and provides an efficient and fast algorithm for inferring couplings and fields, and estimating the cross entropy of the data. To go beyond NMF, we have performed a systematic expansion of \mathcal{S} , based on ideas put forward in the context of the functional renormalization group. Our method automatically resums a class of diagrams, the ‘cactus diagrams’ of Parisi and Potters [29], in addition to the ring diagrams that lead to NMF, which turn out to give a stable inference procedure when couplings are large, or in the presence of biases (fields). After stating our results and sketching their derivation in the case of Ising variables $\sigma = \pm 1$ (a detailed derivation for the Potts variables is given in [47]), we show that our method works well deep in the glass phase of the Sherrington-Kirkpatrick model (SK) [30].

At the lowest order in our expansion, the inferred couplings read

$$J_{ij}^* = -(\mathbf{D} + \mathbf{c})_{ij}^{-1} \quad \forall i < j, \quad (2)$$

where \mathbf{D} is a block diagonal matrix (i.e. $D_{ij} = \delta_{ij} D_i$), that is solved numerically to satisfy

$$L_{ii}^{-1} = (\mathbf{D} + \mathbf{c})_{ii}^{-1} \quad \forall i. \quad (3)$$

Here \mathbf{L} is a diagonal matrix containing the self-correlation of the variables, i.e. $L_{ij} = \delta_{ij}(1 - f_i^2)$. The inferred fields are given by

$$h_i^* = \tanh^{-1}(f_i) - \sum_{j(\neq i)} J_{ij}^* f_j + \frac{D_i f_i}{(1 - f_i^2)^2}, \quad (4)$$

Finally the cross-entropy reads

$$\mathcal{S} = \mathcal{S}_{\text{IM}} - \sum_{i < j} c_{ij} J_{ij}^* + \frac{1}{2} \text{Tr} \ln [\mathbf{K} - \mathbf{L} \mathbf{J}^*], \quad (5)$$

with $\mathcal{S}_{\text{IM}}(\mathbf{f}) = -\sum_i \left[\frac{1-f_i}{2} \ln \left(\frac{1-f_i}{2} \right) - \frac{1+f_i}{2} \ln \left(\frac{1+f_i}{2} \right) \right]$ the cross-entropy of the independent model. Evaluating Eqs. (2-5) at \mathbf{f}^M and \mathbf{p}^M gives the RMF solution of the inference problem. The NMF is recovered when \mathbf{D} is set to zero. The equations defining \mathbf{D} are $N \times (q-1)^2$ coupled equations, and a simple iterative scheme solves it in a matter of seconds or minutes depending on the values of N and q [47].

To obtain Eqs. (2-5), we introduce a temperature-like parameter β in front of \mathbf{J} in the partition function [18, 19]. Setting $\beta = 0$ decouples the variables and gives \mathcal{S}_{IM} , while we aim to solve the case $\beta = 1$. Introducing the Gibbs free energy \mathcal{G} as the Legendre transform of $\ln Z$ with respect to \mathbf{h} , we can write down an exact equation for \mathcal{G} , known as the Wetterich equation in statistical field theory [31],

$$\partial_\beta \mathcal{G}[\mathbf{f}, \mathbf{J}] = \sum_{i < j} J_{ij} c_{ij} + \sum_{i < j} J_{ij} f_i f_j, \quad (6)$$

where $(\mathbf{c}^{-1})_{ij} = -\delta^2 \mathcal{G} / \delta f_i \delta f_j \equiv -\mathcal{G}_{ij}^{(2)}$ is the inverse correlation function of a model with frequencies \mathbf{f} and couplings \mathbf{J} . This equation has been the starting point to non-perturbatively tackle a variety of problems stemming from quantum and statistical field theories [32], with recent development for classical and quantum lattice models [33-35].

Solving Eq. (6) exactly is as hard as computing the partition function directly, and one has to resort to approximate solutions. One could expand in powers of β to straight-forwardly recover the high-temperature expansion of [18, 19], followed by a Legendre transform with respect to \mathbf{J} to recover the results of [20], see [36]. To go beyond the high-temperature expansion, we resort to the so-called ‘loop expansion’ in field theory [37]. In the context of Eq. (6), it amounts to expanding the Gibbs free energy in powers of a fictitious parameter ε [38],

$$\mathcal{G} = \mathcal{G}_{\text{NMF}} + \varepsilon \mathcal{G}_1 + \dots \Rightarrow \mathbf{c} = \mathbf{c}^{\text{NMF}} + \varepsilon \mathbf{c}^{\text{NMF}} \mathcal{G}_1^{(2)} \mathbf{c}^{\text{NMF}} + \dots \quad (7)$$

where the NMF functional reads $\mathcal{G}_{\text{NMF}} = \mathcal{S}_{\text{IM}} + \beta \sum_{i < j} J_{ij} f_i f_j$ and the corresponding correlation function is $\mathbf{c}^{\text{NMF}} = (\mathbf{L}^{-1} - \beta \mathbf{J})^{-1}$. Inserting Eq. (7) into Eq. (6) leads to a tower of equations for the \mathcal{G}_n that

can be solved order by order explicitly. This leads to a straightforward procedure to generate all terms in this expansion, leading to simple diagrammatics that are well known in field theory, see [47].

Once the Gibbs free energy has been computed at a given order in ε , one possibility for inferring couplings would be to try to find the couplings \mathbf{J}^* that satisfy the equation $\mathcal{G}^{(2)}[\mathbf{f}, \mathbf{J}^*] = -(\mathbf{c}^M)^{-1}$. At order zero in the expansion, this gives back the NMF. An interesting remark is that in the direct problem, finding \mathbf{c} given \mathbf{J} , one has $c_{ii} \neq L_{ii}$, which has to be cured in an ad-hoc way, an approach followed by the adaptive TAP equation [39] and similar works [28, 40] or works based on the Bethe free energy [24, 25]. Because we instead perform the second Legendre transform, our results are free from such ambiguities.

To do this at first order in our ε expansion, we need to solve ($\varepsilon = \beta = 1$)

$$\left. \frac{\delta \mathcal{G}[\mathbf{f}, \mathbf{J}]}{\delta J_{ij}} \right|_{\mathbf{J}^*} = p_{ij} \Rightarrow c_{ij} = (\mathbf{L}^{-1} - \mathbf{J}^*)_{ij}^{-1} \quad \forall i < j. \quad (8)$$

This equation cannot be inverted directly (in a matrix sense) because we do not have an equation for $i=j$. To circumvent this problem we introduce a matrix \mathbf{D} such that

$$\mathbf{c} + \mathbf{D} = (\mathbf{L}^{-1} - \mathbf{J}^*)^{-1} \quad (9)$$

is true in the matrix sense, allowing for the inversion, and leading directly to the lowest order of the RMF, Eqs. (2–3). Some intuition of the effect of \mathbf{D} can be gained by looking at its high-temperature expansion, see [47]. The calculation can be easily continued to second order in ε , and to third order for Ising variables, although it becomes gradually more tedious, the number of diagrams, and terms, increasing rapidly [36].

Tests on the Sherrington-Kirkpatrick model- In order to test our approach, we analyze the standard SK model, which consists of N spins interacting with random gaussian couplings J_{ij} of zero mean and standard deviation $\sigma_J = J/\sqrt{N}$. We have performed Monte-Carlo simulations of an SK model with $N=10$ spins for $\sigma_J \in [0.1, 0.9]$ in presence of a random gaussian magnetic field h_i , of zero mean and standard deviation $\sigma_h=0.3$. As the high temperature expansion becomes exact as $N \rightarrow \infty$, a small number of spins is actually an interesting test case. We have generated various sets of $M=100$ and $M=10000$ spin configurations, for 100 realizations of the disorders per σ_J . (Exact computations, that are feasible for $N=10$, showed that results at $M=10000$ are close to that of the perfect sampling regime.) The corresponding \mathbf{f}^M and \mathbf{c}^M were calculated and used as input in Eq. (2) to obtain the inferred fields and couplings \mathbf{h}^* and \mathbf{J}^* . Note that our simulations were not necessarily thermalized in the glass phase, implying possibly strongly biased evaluation of the averages.

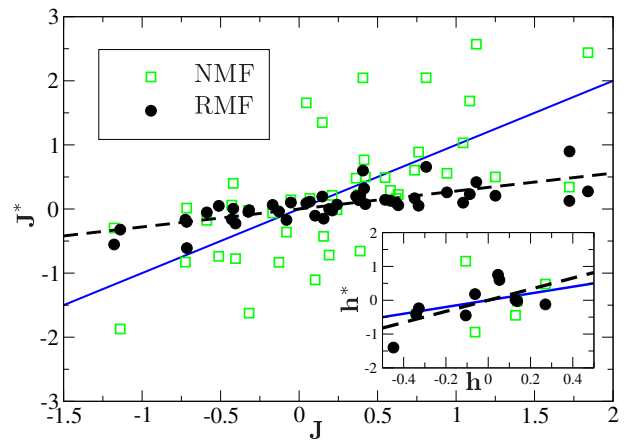


FIG. 1. Scatter plot of inferred (y-axis) versus true couplings (x-axis), for one realization of \mathbf{J} and \mathbf{h} at $\sigma_J=0.7$, $M=100$. Black circles: RMF results; green empty squares: NMF. Inset: inferred (y-axis) versus true fields (x-axis), same legend. Dashed lines are linear regressions of the RMF results with slope 0.28 (1.65) for the couplings (fields). Blue line has slope 1. Some NMF points are out of the graph range.

In the last few years, it has been understood that in presence of a magnetic field, standard inference approaches, such as the TAP equation or Bethe approximation, do not converge (i.e. give complex results) [23], whereas the NMF and the approximation of [20] break down in the glassy phase ($J \gtrsim 1$). We have checked that this also happens here, and we will therefore only show comparisons between the RMF and NMF inference for clarity.

We typically find that NMF breaks down for $\sigma_J \gtrsim 0.3$, in the sense that the couplings and fields inferred may take values larger than the real ones by orders of magnitude, and that they are quite uncorrelated with the value of the real couplings. On the other hand, our simple RMF approximation works very well to infer the order of magnitude of the couplings and the fields, that are highly correlated with the true ones, even deep in the glass phase, see an illustration of this in Fig. 1.

A striking feature (that will turn to our advantage) is that the inferred couplings are typically smaller than the true ones: the inferred couplings are proportional to the true ones, with a very good Pearson correlation r_J (see caption of Fig. 2), while the prefactor depends on the realization of the disorder. To quantify the success or failure of NMF and RMF, we have decided to use this Pearson correlation instead of the more common relative error, defined by $\Delta_J^2 = \sum_{i < j} (J_{ij}^* - J_{ij})^2 / \sum_{i < j} J_{ij}^2$. The reason for our choice is that we found that the deeper in the glass phase, the smaller the inferred RMF couplings were, and the bigger the NMF couplings, so that the RMF relative error artificially saturates at one, while the NMF relative error explodes, see [47]. The Pearson correlations of the fields and couplings are shown in Fig. 2.

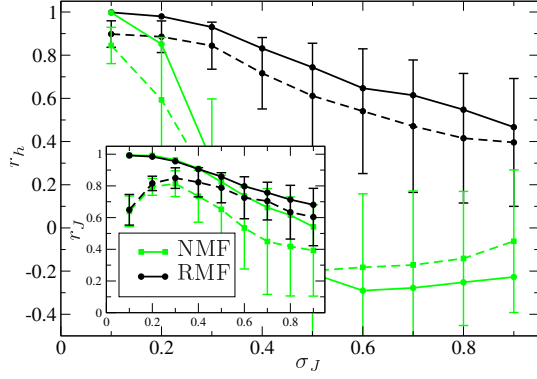


FIG. 2. Pearson correlations r_h between inferred fields from RMF (black) and NMF (green) and the true fields, averaged over for a hundred realizations of \mathbf{J} and \mathbf{h} , with $r_h = \sum_i (h_i - \langle h_i \rangle)(h_i^* - \langle h_i^* \rangle) / N \sigma_h \sigma_{h^*}$, where $\langle h \rangle$ and σ_h are the mean and standard deviation of the fields for a single realization of the disorder. Full lines (resp. dashed lines) correspond to simulations with $M = 10000$ (resp. 100). Inset: average Pearson correlation for the couplings r_J (with definition similar to that of r_h) for RMF and NMF. Error bars are shown only for $M = 100$ (but are similar for $M = 1000$) and correspond to plus and minus one standard deviation of r_h and r_J .

The RMF fields are by far much better than that of NMF, while for the couplings, some improvement is found over NMF. But once more, one has to keep in mind that NMF couplings, while correlated with the true couplings, typically have very large values for $\sigma_J \gtrsim 0.4$, assuming the corresponding \mathbf{c}^M is invertible, which might not be the case.

We stress that we did not use any pseudocount or regularization here, and that although \mathbf{c}^M might not be invertible due to imperfect sampling, in particular in the glassy phase for small $M \simeq 100$, we could always converge the matrix \mathbf{D} , that effectively acts as a regularizer for the matrix \mathbf{c}^M . This feature is very striking, especially deep in the glass phase, where the data are very polarized and many pairs of spin values are never observed, leading to either rank-deficient, or nearly singular, \mathbf{c}^M matrices. In the first case the NMF fails (the corresponding disorder realizations were ignored to compute r_J^{NMF}), and in the second case much too large couplings are obtained for NMF. We see in Fig. 1 that the effect of the \mathbf{D} matrix is to describe more of the data features with fields and less with couplings (see the slopes of the linear fits), instead of explaining missing data by very large couplings as NMF tends to do. See [41] for an illustration of this issue in machine learning.

The validity of the inferred couplings and fields can be measured using the energy $E(\mathbf{J}, \mathbf{h}) = -\sum_i h_i \sigma_i - \sum_{i < j} J_{ij} \sigma_i \sigma_j$, which were calculated from an independent set of $M=1000$ Monte-Carlo sampled configurations $\{\mathcal{C}\}$ from the original model (\mathbf{J}, \mathbf{h}) , and evaluated with the inferred NMF and RMF couplings $(\mathbf{J}^*, \mathbf{h}^*)$. The

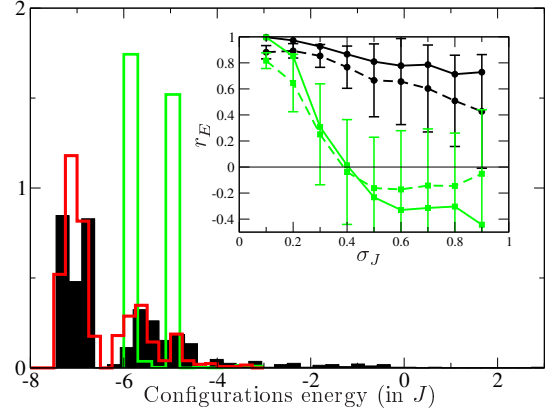


FIG. 3. Energy distribution $E(\mathbf{J}, \mathbf{h})$ of 1000 spin configurations sampled from the true distribution (\mathbf{J}, \mathbf{h}) , $\{\mathcal{C}\}$ (red histogram), RMF inference $(\mathbf{J}^*, \mathbf{h}^*)$ with $M=100$, $\{\mathcal{C}_{\text{RMF}}\}$ (black), and NMF inference with $M=100$, $\{\mathcal{C}_{\text{NMF}}\}$ (green). Inset : Pearson correlation r_E of the energy (see text) obtained from the true and inferred couplings and fields, averaged over the realization of disorder. Same legend as Fig. 2.

inset of Fig. 3 shows the Pearson correlations between $E(\mathbf{J}, \mathbf{h})$ and $E(\mathbf{J}^*, \mathbf{h}^*)$ for $\{\mathcal{C}\}$, averaged over the disorder realizations, as a function of σ_J . It clearly demonstrates the validity of RMF, and the poor results of NMF, in the glass phase. Using the configurations drawn with the inferred RMF couplings and fields $\{\mathcal{C}_{\text{RMF}}\}$, one can also our inference gives rise to meaningful frequencies and correlations, see [47].

One of the main interest of the inference is the ability to generate new configurations, which have high probabilities (i.e. low energy) in the real model [42]. Using the RMF couplings $(\mathbf{J}^*, \mathbf{h}^*)$, we have generated a thousand configurations $\{\mathcal{C}_{\text{RMF}}\}$ via Monte-Carlo sampling. To test whether these configurations would have a high probability, one can compare the energy of each configuration of $\{\mathcal{C}_{\text{RMF}}\}$ in the original model (\mathbf{J}, \mathbf{h}) to the energy of typical configurations drawn from the real model. We find that the configurations $\{\mathcal{C}_{\text{RMF}}\}$ generically have low energy in the real model, i.e., they are configurations that are typical or the original model. Because the NMF has very wrong fields, the corresponding configurations $\{\mathcal{C}_{\text{NMF}}\}$ are strongly polarized and NMF fails to find the correct low-energy states. Fig. 3 shows an example of these energy distributions, for the couplings inferred from the same realization of (\mathbf{J}, \mathbf{h}) than in Fig. 1.

Conclusion- We have introduced the resummed mean-field approximation for the inference problem in the context of Potts (and Ising) variables, which is based on an exact equation for the Gibbs free energy. At the lowest non-trivial order, we obtained a simple analytical expression for the couplings and the fields as functions of the correlations and frequencies. The main difference compared to other approaches is the introduction of the matrix \mathbf{D} , which has to be solved numerically, although at a

small cost. Our expansion can be pursued in a principled way, and the second and third order are straight-forward to obtain [36].

We have tested the method on the SK model and shown that RMF works well even in the glassy phase, in particular in presence of a magnetic field, where other methods break down. The inferred couplings and fields are well correlated with the real ones, and of the correct order of magnitude, although the couplings tend to be smaller than expected. A striking result is that we do not need to include a pseudocount for small sampling, even when the correlation matrix c^M is not invertible, which is a clear improvement upon mean-field. This feature is crucial for practical applications, and we expect this, together with the fact that the inference is reliable even for large couplings, to pave the way for systematic applications to very large datasets, and/or datasets with units assuming a large number of possible states. We have also demonstrated that the inference performed by our method is consistent with the original model at the level of the probabilities of single configurations, a feature that could have important implications in bio-informatics [42, 43].

The method presented here can be easily generalized to other kind of variables, e.g. continuous variables, along the lines of [33], or to restricted Boltzmann machines following [44]. The main requirement for the method to be valid is that there exist a well defined Independent Model Gibbs functional \mathcal{G}_{IM} . One could also imagine dealing with quantum variables in the context of quantum inference, following the calculation of [45].

H.J. was funded by the Agence Nationale de la Recherche Coevstat project (ANR-13-BS04-0012-01), and acknowledges support from the Laboratoire de Physique Statistique de l'École Normale Supérieure de Paris. A.R. was funded by ANR "ArtiQ" project. We thank C.K. Fisher for stimulating discussions, and F. Krzakala and R. Monasson for important suggestions.

-
- [1] G. Tkacik, O. Marre, T. Mora, D. Amodei, M. J. Berry and W. Bialek, *J. Stat. Mech.* **2013**, P03011 (2013).
 - [2] O. Marre, S. El Boustani, Y. Frégnac, and A. Destexhe, *Phys. Rev. Lett.* **102**, 138101 (2009).
 - [3] Y. Roudi, J. Tyrcha, and J. Hertz, *Phys. Rev. E* **79**, 051915 (2009).
 - [4] M. Weigt, R. A. White, H. Szurmant, J. A. Hoch, and T. Hwa, *PNAS* **106**, 67 (2009).
 - [5] F. Morcos, A. Pagnani, B. Lunt, A. Bertolino, D. S. Marks, C. Sanders, R. Zecchina, J. N. Onuchic, T. Hwa and M. Weigt, *Proc. Nat. Acad. Sci.* **108**, E1293 (2011).
 - [6] M. Ekeberg, C. Lövkvist, Y. Lan, M. Weigt, and E. Aurell, *Physical Review E* **87**, 012707 (2013).
 - [7] W. Bialek, A. Cavagna, I. Giardina, T. Mora, E. Silvestri, M. Viale, and A. M. Walczak, *PNAS* **109**, 4786 (2012).
 - [8] S. S. Borysov, Y. Roudi, and A. V. Balatsky, *arXiv:1504.02280* (2015).
 - [9] E. T. Jaynes, *Phys. Rev.* **106**, 620 (1956).
 - [10] S. Cocco and R. Monasson, *J. Stat. Phys.* **147**, 252 (2012).
 - [11] D. Ackley, G. E. Hinton and T. J. Sejnowski, *Cognitive Science* **9**, 147 (1985).
 - [12] P. Ravikumar, M. J. Wainwright, and J. D. Lafferty, *The Annals of Statistics* **38**, 1287 (2010).
 - [13] E. Aurell and M. Ekeberg, *Phys. Rev. Lett.* **108**, 090201 (2012).
 - [14] S. Cocco and R. Monasson, *Phys. Rev. Lett.* **106**, 090601 (2011).
 - [15] T. Broderick, M. Dudik, G. Tkacik, R. E. Schapire, and W. Bialek, *arxiv:0712.2437*
 - [16] J. Sohl-Dickstein, P. B. Battaglino, and M. R. DeWeese, *Phys. Rev. Lett.* **107**, 220601
 - [17] U. Ferrari, *arxiv:1507.04254*
 - [18] T. Plefka, *J. Phys. A* **15**, 1971 (1982).
 - [19] A. Georges and J. S. Yedidia, *J. Phys. A* **24**, 2173 (1991).
 - [20] V. Sessak and R. Monasson, *J. Phys. A* **42**, 055001 (2009).
 - [21] M. Mézard and T. Mora, *Journal of Physiology* **103**, 107 (2009).
 - [22] H. C. Nguyen and J. Berg, *J. Stat. Mech.* **2012** Pxxxxx.
 - [23] F. Ricci-Tersenghi, *J. Stat. Mech.* (2012) P08015.
 - [24] J. Raymond and F. Ricci-Tersenghi, *Phys. Rev. E* **87**, 052111 (2013).
 - [25] J. Raymond and F. Ricci-Tersenghi, *IEEE ICC'13*, 1429 (2013).
 - [26] J. P. Barton, S. Cocco, E. De Leonardis and R. Monasson, *Phys Rev E* **90**, 012132 (2014).
 - [27] H. C. Nguyen and J. Berg, *Phys. Rev. Lett.* **109**, 050602 (2012).
 - [28] H. Huang and Y. Kabashima, *Phys. Rev. E* **87**, 062129 (2013).
 - [29] G. Parisi and M. Potters, *J. Phys. A* **28**, 5267 (1995).
 - [30] D. Sherrington and S. Kirkpatrick, *Phys. Rev. Lett.* **35**, 1792 (1975).
 - [31] C. Wetterich, *Phys. Lett. B* **301**, 90 (1993).
 - [32] J. Berges, N. Tetradis and C. Wetterich, *Phys. Rep.* **363**, 223 (2002).
 - [33] T. Machado and N. Dupuis, *Phys. Rev. E* **82**, 041128 (2010).
 - [34] A. Rançon and N. Dupuis, *Phys. Rev. B* **83**, 172501 (2011).
 - [35] A. Rançon and N. Dupuis, *Phys. Rev. B* **84**, 174513 (2011).
 - [36] A. Rançon and H. Jacquin, in preparation.
 - [37] J. Zinn-Justin, (Oxford, Clarendon Press, 1989).
 - [38] D. Litim and J. Pawłowski, *Phys. Rev. D* **66**, 025030 (2002).
 - [39] M. Oppen and O. Winther, *Phys. Rev. E* **64**, 056131 (2001).
 - [40] H. Kiwata, *Phys. Rev. E* **89**, 062135 (2014).
 - [41] C. K. Fisher, *arXiv:1409.7074v1* (2014).
 - [42] M. Socolich et al, *Nature* **437**, 512 (2005).
 - [43] W. P. Russ et al, *Nature* **437**, 579 (2005).
 - [44] M. Gabrié, E. W. Tramel and F. Krzakala, *arXiv:1506.02914* (2015).
 - [45] A. Rançon, *Phys. Rev. B* **89**, 214418 (2014).
 - [46] S. Cocco, R. Monasson and M. Weigt, *PLoS Comput. Biol.* **9** (2013).
 - [47] See supplemental materials.

SUPPLEMENTAL MATERIALS

Expansion of the Gibbs free energy and cross-entropy

Here we derive the expansion that leads to the RMF. We start by considering a Potts model with q possible states for each unit, i.e. $\sigma_{ia} = \delta_{a,a_i}$, where $a_i = 1 \dots q$ represents the q possible states on site i . The Ising case of $q=2$, for which it is customary to set $\sigma_i = -1, 1$ is treated in Appendix B. Switching from Potts to Ising only requires to change the expression for the independent model entropy, and introducing additional summations over Potts indices, whereas the generalization to different number of states per site (i.e. $q \rightarrow q_i$) is straightforward.

Definitions

The Gibbs potential \mathcal{G} is the first Legendre transform of $\ln Z[\mathbf{h}, \mathbf{J}]$ with respect to the fields

$$\begin{cases} \mathcal{G}[\mathbf{f}, \mathbf{J}] = \ln Z[\mathbf{h}^*[\mathbf{f}], \mathbf{J}] - \sum_{\alpha} h_{\alpha}^* f_{\alpha} , \\ \mathbf{h}^* \text{ such that } \left. \frac{\delta \ln Z[\mathbf{h}, \mathbf{J}]}{\delta h_{\alpha}} \right|_{\mathbf{h}^*} = f_{\alpha} , \end{cases} \quad (10)$$

where too alleviate the notations, we will often use greek letters to combine both the sites (i, j, k, \dots) and Potts (a, b, c, \dots) indices, that is $\alpha = (i, a)$, $\beta = (j, b)$, $\gamma = (k, c)$, etc. Here, \mathbf{h}^* is the stationary point, and a subsequent Legendre transform with respect to couplings will generate the cross-entropy of the data \mathcal{S} ,

$$\begin{cases} \mathcal{S}[\mathbf{f}, \mathbf{p}] = \mathcal{G}[\mathbf{f}, \mathbf{J}^*] - \sum_{i < j, ab} J_{ia,jb}^* p_{ia,jb} . \\ \mathbf{J}^* \text{ such that } \left. \frac{\delta \mathcal{G}[\mathbf{f}, \mathbf{J}]}{\delta J_{\alpha\beta}} \right|_{\mathbf{J}^*} = p_{\alpha\beta} . \end{cases} \quad (11)$$

The sought for fields and couplings \mathbf{h}^* and \mathbf{J}^* are then found by looking for the stationary points of \mathcal{S} ,

$$h_{\alpha}^* = -\frac{\delta \mathcal{S}[\mathbf{f}, \mathbf{p}]}{\delta f_{\alpha}} , \quad J_{\alpha\beta}^* = -\frac{\delta \mathcal{S}[\mathbf{f}, \mathbf{p}]}{\delta p_{\alpha\beta}} , \quad (12)$$

and the inference problem is solved when evaluating all these objects in the data marginals \mathbf{f}^M and \mathbf{p}^M .

Following [18–20] we introduce the temperature-dependent free energy

$$\mathcal{F}(\beta) = \ln \left[\sum_{\sigma} \exp \left(\sum_{\alpha} h_{\alpha} \sigma_{\alpha} + \beta \sum_{\alpha, \beta} J_{\alpha\beta} \sigma_{\alpha} \sigma_{\beta} \right) \right] . \quad (13)$$

The summation over $\alpha, \beta = ia, jb$ is done over $i < j$. Note that there is an ambiguity in the way of defining

fields and couplings and one has to fix a gauge to remove it. A simple way to see this issue is to consider the one- and two-point functions

$$f_{\alpha} = \langle \sigma_{\alpha} \rangle , \quad \text{and} \quad p_{\alpha\beta} = \langle \sigma_{\alpha} \sigma_{\beta} \rangle . \quad (14)$$

They have to satisfy a set of simple constraints:

$$\sum_{a=1}^q f_{ia} = 1, \quad \text{and} \quad \begin{cases} \sum_{a=1}^q p_{ia,jb} = f_{jb}, \\ \sum_{b=1}^q p_{ia,jb} = f_{ia}. \end{cases} \quad (15)$$

When trying to infer the fields and couplings we will find that we have too many variables with respect to the set of equations that fix their values. A simple way to fix this is to choose fields and couplings such that

$$\begin{aligned} h_{iq} &= 0 \quad \forall i , \\ J_{ia,jq} &= J_{iq,jb} = J_{iq,jq} = 0 \quad \forall i < j, a, b. \end{aligned} \quad (16)$$

Note that $J_{ia,ib} = 0 \quad \forall i, a, b$. Other choices are possible, see for example [46], and the calculation can easily be repeated with different gauge fixations, only impacting the independant model Gibbs free-energy in Eq. (21). In the following, all summations over Potts indices will thus run from 1 to $q-1$ unless specified otherwise. Finally, the introduction of the β parameter couples \mathbf{J} to $\beta \mathbf{p}$ instead of \mathbf{p} , and one has to modify the definition of the second Legendre transform in Eq. (11) accordingly.

These technicalities aside, one easily sees that setting $\beta = 0$ decouples the variables and retrieves the independent spin model, and the model of interest is obtained for $\beta = 1$. We are interested in calculating the temperature dependent Gibbs potential

$$\mathcal{G}(\beta) = \mathcal{F}(\beta) - \sum_{\alpha} h_{\alpha}^* f_{\alpha} , \quad (17)$$

which is the Legendre transform of the Free energy, as stated above. Here \mathcal{F} depends on the fields h_{α} whereas \mathcal{G} depends on the magnetization $f_{\alpha} = \partial \mathcal{F} / \partial h_{\alpha}$. Standard properties of the Legendre transforms show that

$$h_{\alpha}^*(\beta) = -\frac{\delta \mathcal{G}(\beta)}{\delta f_{\alpha}} , \quad (c^{-1}(\beta))_{\alpha\beta} = -\frac{\delta^2 \mathcal{G}(\beta)}{\delta f_{\alpha} \delta f_{\beta}} , \quad (18)$$

For future convenience we introduce the notation

$$\mathcal{G}_{\alpha_1 \dots \alpha_n}^{(n)}(\beta) = \frac{\delta^n \mathcal{G}(\beta)}{\delta f_{\alpha_1} \dots \delta f_{\alpha_n}} , \quad \forall n \geq 2 . \quad (19)$$

Differentiating $\mathcal{G}(\beta)$ with respect to β we obtain an exact equation which is the starting point of our expansion

$$\partial_{\beta} \mathcal{G}(\beta) = \frac{1}{2} \text{Tr} (\mathbf{J} \mathbf{c}(\beta)) + \frac{1}{2} \mathbf{f}^T \mathbf{J} \mathbf{f} , \quad (20)$$

where $c_{\alpha\beta}(\beta)$ is given by Eq. (18). The initial condition for this partial differential equation is given by $\mathcal{G}(\beta =$

0), which corresponds to the (exact) Gibbs potential of the independent model (IM), \mathcal{S}_{IM} which for our choice of gauge reads

$$\mathcal{S}_{\text{IM}}[\mathbf{f}] = - \sum_{ia} f_{ia} \ln f_{ia} - \sum_i \left(1 - \sum_a f_{ia}\right) \ln \left(1 - \sum_a f_{ia}\right). \quad (21)$$

The second derivative of this functional with respect to frequencies is of particular interest for our calculation and we define

$$L_{ia,jb}^{-1} = - \frac{\delta^2 \mathcal{S}_{\text{IM}}[\mathbf{f}]}{\delta f_{ia} \delta f_{jb}} = \delta_{ij} \left[\frac{1}{f_{ia}} \delta_{ab} + \frac{1}{1 - \sum_b f_{ib}} \right], \quad (22)$$

the inverse of which is simply (when $i = j$) the self correlation of a Potts variable

$$L_{ia,jb} = \delta_{ij} f_{ia} (\delta_{ab} - f_{ib}). \quad (23)$$

We see that the \mathbf{L} function, that will enter the diagrams of our expansion is diagonal in the site sector (indices (i, j)), but not in the sector of the Potts states (indices (a, b)), which increases the complexity of the calculations when compared to the Ising, $q = 2$, case.

The third and higher-order derivatives of \mathcal{S}_{IM} are calculated as

$$\gamma_{\alpha_1 \dots \alpha_n}^{(n)} = - \frac{\delta^n \mathcal{S}_{\text{IM}}}{\delta f_{\alpha_1} \dots \delta f_{\alpha_n}}, \quad (24)$$

They are local in the site variables, but not in the Potts variables, which lead us to define:

$$\begin{aligned} \gamma_{i_1 a_1, \dots, i_n a_n}^{(n)} &= \delta_{i_1 i_2} \dots \delta_{i_{n-1} i_n} \gamma_{i_1; a_1, \dots, a_n}^{(n)}[\mathbf{f}] \\ \frac{\gamma_{i; a_1, \dots, a_n}^{(n)}[\mathbf{f}]}{(n-2)!} &= \frac{(-1)^n}{f_{ia_1}^{n-1}} \prod_{k=2}^n \delta_{a_1 a_k} + \frac{1}{(1 - \sum_a f_{ia})^{n-1}} \end{aligned} \quad (25)$$

These quantities will be the vertices of the diagrams of our expansion.

Gibbs free energy up to second order : First order

To organize our expansion beyond mean-field, we introduce a small parameter ε (set to one at the end of the calculation) and assume that $\mathcal{G}(\beta)$ can be formally expanded in ε as

$$\mathcal{G}(\beta) = \sum_{n=0}^{\infty} \varepsilon^n \mathcal{G}_n(\beta). \quad (26)$$

We also assume that the first term in the right-hand side of Eq. (20) is of order ε , that is we rewrite it as

$$\partial_\beta \mathcal{G}(\beta) = \frac{\varepsilon}{2} \text{Tr}(\mathbf{J} \mathbf{c}(\beta)) + \frac{1}{2} \mathbf{f}^T \mathbf{J} \mathbf{f}. \quad (27)$$

We also have that $\mathcal{G}(\beta=0) = \mathcal{G}_0(\beta=0) = \mathcal{S}_{\text{IM}}$ (this is consistent with the solution of Eq. (27) to all order in ε). This in turn ensures that the lowest order term allows to recover the mean-field result (see below). We can now expand both sides of Eq. (27) in ε and solve each order in ε iteratively. In particular, one needs to expand $\mathbf{c}(\beta)$ in ε , which reads to order ε^2 ,

$$\mathbf{c} = \mathbf{c}_0 + \varepsilon \mathbf{c}_0 \mathcal{G}_1^{(2)} \mathbf{c}_0 + \varepsilon^2 \mathbf{c}_0 \left(\mathcal{G}_2^{(2)} + \mathcal{G}_1^{(2)} \mathbf{c}_0 \mathcal{G}_1^{(2)} \right) \mathbf{c}_0 + \dots, \quad (28)$$

where we have suppressed the dependence on β for readability. We emphasize that we do not perform any expansion in powers of β , and β here serves only as a book-keeping parameter to build the ε expansion, i.e. to generate the exact equation (20).

To lowest order in ε , we thus have after a trivial integration with respect to β :

$$\mathcal{G}_0(\beta) = \mathcal{G}_{\text{NMF}}(\beta) \equiv \mathcal{S}_{\text{IM}} + \frac{\beta}{2} \mathbf{f}^T \mathbf{J} \mathbf{f}. \quad (29)$$

Eq. (29) is the mean-field result for the Gibbs potential, and the corresponding correlation function reads after two differentiations with respect to \mathbf{f} ,

$$\mathbf{c}_0(\beta) = \mathbf{c}^{\text{NMF}}(\beta) = (\mathbf{L}^{-1} - \beta \mathbf{J})^{-1}. \quad (30)$$

Eq. (27) to next order in ε reads

$$\partial_\beta \mathcal{G}_1(\beta) = -\partial_\beta \left[\frac{1}{2} \text{Tr} \ln(\mathbf{L}^{-1} - \beta \mathbf{J}) \right], \quad (31)$$

This last equation can again be integrated easily with respect to β . To order ε , the Gibbs potential is thus given by

$$\begin{aligned} \mathcal{G}(\beta) &= \mathcal{S}_{\text{IM}} + \frac{\beta}{2} \mathbf{f}^T \mathbf{J} \mathbf{f} \\ &\quad - \frac{\varepsilon}{2} \text{Tr} \left[\ln(\mathbf{L}^{-1} - \beta \mathbf{J}) - \ln \mathbf{L}^{-1} \right] + \mathcal{O}(\varepsilon^2), \end{aligned} \quad (32)$$

One can check that the expansion to order β^2 gives the TAP equations with the Onsager reaction term.

Second order

To pursue the calculation to order ε^2 , it is useful to introduce first the following notation:

$$\mathbf{G} = (\mathbf{L}^{-1} - \beta \mathbf{J})^{-1} - \mathbf{L}, \quad (33)$$

which will be the propagator in the diagrams we will construct in the following.

Eq. (27) to order ε^2 reads

$$\partial_\beta \mathcal{G}_2(\beta) = \frac{1}{2} \text{Tr} \left(\mathbf{J} \mathbf{c}_0(\beta) \mathcal{G}_1^{(2)}(\beta) \mathbf{c}_0(\beta) \right), \quad (34)$$

$$\mathcal{G}_2 = -\frac{1}{8} \text{diagram} + \frac{1}{12} \left(\text{diagram} + 3 \text{diagram} \right)$$

FIG. 4. Diagrammatic representation of the second order correction to the Gibbs potential. Grey blobs with n dots represent $\gamma^{(n)}$ vertices. Black dots represent summation over the indices, full lines represent $G(\beta)$ and dotted lines represent L .

with

$$\begin{aligned} \mathcal{G}_{1,\alpha\beta}^{(2)}(\beta) &= -\frac{1}{2} \sum_{\gamma,\delta} \gamma_{\alpha\beta\gamma\delta}^{(4)} [c_{0,\gamma\delta}(\beta) - L_{\gamma\delta}] \\ &+ \frac{1}{2} \sum_{\gamma\delta\mu\nu} \gamma_{\alpha\gamma\delta}^{(3)} [c_{0,\gamma\mu}(\beta) c_{0,\delta\nu}(\beta) - L_{\gamma\mu} L_{\delta\nu}] \gamma_{\mu\nu\beta}^{(3)}. \end{aligned} \quad (35)$$

One then readily realizes that Eq. (34), and in fact all subsequent orders, can be rewritten as a total derivative with respect to β , and one obtains

$$\begin{aligned} \mathcal{G}_2(\beta) &= -\frac{1}{8} \sum_{\alpha\beta\gamma\delta} G_{\alpha\beta} \gamma_{\alpha\beta\gamma\delta}^{(4)} G_{\gamma\delta} \\ &+ \frac{1}{12} \sum_{\alpha\beta\gamma\delta\mu\nu} \gamma_{\alpha\gamma\mu}^{(3)} (G_{\alpha\beta} G_{\gamma\delta} G_{\mu\nu} + 3L_{\alpha\beta} G_{\gamma\delta} G_{\mu\nu}) \gamma_{\beta\delta\nu}^{(3)}. \end{aligned} \quad (36)$$

This expression can be represented in a diagrammatic way as shown in figure 4. Note that there are here well-known diagrammatic rules to compute the factors and signs in front of each terms. We thus expect that our calculation can be pushed much further analytically or even using symbolic calculation programs in the future.

Cross-entropy at order ε

In order to have a consistent expansion we have to define the off-diagonal part of the connected correlation with an ε factor.

$$c_{ia,jb} = L_{ia,jb} + \varepsilon \tilde{c}_{ia,jb} \quad (37)$$

where the \tilde{c} matrix is zero on the $i = j$ blocks.

Starting from our expansion of the Gibbs free energy (at $\beta = 1$), and plugging it in Eq. (11) defining the optimal couplings we obtain

$$\tilde{c}_{\alpha\beta} = F_{\alpha\beta}^{(1)}[\mathbf{J}^*] + \varepsilon F_{\alpha\beta}^{(2)}[\mathbf{J}^*] + \dots \quad (38)$$

where

$$F_{ia,jb}^{(n)}[\mathbf{J}] = \frac{\delta \mathcal{G}_n}{\delta J_{ia,jb}} \quad \forall i < j, ab. \quad (39)$$

We look for the ε expansion of \mathbf{J}^* that solves Eq. (11),

$$\mathbf{J}^* = \mathbf{J}^{(1)} + \varepsilon \mathbf{J}^{(2)} + \dots \quad (40)$$

where the $\mathbf{J}^{(n)}$ are functionals of both \mathbf{f} and $\tilde{\mathbf{c}}$. Note that we loosely use the notations \mathbf{J} , or $\mathbf{J}^{(n)}$, to denote the symmetrized matrices gathering the $J_{ia,jb}$ for $i < j$, with zeros on the diagonal, but keep in mind that the only free variables here are the $J_{ia,jb}$ for $i < j$.

The expansion is done by plugging Eq. (40) into Eq. (38), expand in ε and match term by term in power of ε . We then obtain ($i \neq j$)

$$\begin{aligned} \tilde{c}_{ia,jb} &= F_{ia,jb}^{(1)}[\mathbf{J}^{(1)}], \\ 0 &= \sum_{\gamma\delta} \mathbf{J}_{\gamma\delta}^{(2)} \left. \frac{\delta F_{ia,jb}^{(1)}}{\delta J_{\gamma\delta}} \right|_{\mathbf{J}^{(1)}} + F_{ia,jb}^{(2)}[\mathbf{J}^{(1)}], \\ &\vdots \end{aligned} \quad (41)$$

We now proceed to solve \mathbf{J} to order ε .

Starting from the first order approximation of Eq. (32), and Eq. (11) we get

$$\tilde{c}_{ia,jb} = \left(\mathbf{L}^{-1} - \mathbf{J}^{(1)} \right)_{ia,jb}^{-1} \quad \forall i < j, ab. \quad (42)$$

These are $N(N-1)/2 \times (q-1)^2$ equations for the parameters $J_{ia,jb}^{(1)}$ for $i < j$. To have a more explicit formula for the $\mathbf{J}^{(1)}$ matrix we complement these equations by $N \times (q-1)^2$ equations

$$0 = \left(\mathbf{L}^{-1} - \mathbf{J}^{(1)} \right)_{ia,ib}^{-1} - L_{ia,ib} - D_{ia,ib} \quad (43)$$

where \mathbf{D} is an unknown block diagonal matrix, i.e. $D_{ia,jb} = \delta_{ij} D_{ia,ib}$. With this definition of \mathbf{D} , we can now invert Eq. (42) to find

$$J_{ia,jb}^{(1)} = -(\mathbf{L} + \tilde{\mathbf{c}} + \mathbf{D})_{ia,jb}^{-1} \quad \forall i < j, ab, \quad (44)$$

where \mathbf{D} is defined through:

$$L_{ia,ib}^{-1} - (\mathbf{L} + \tilde{\mathbf{c}} + \mathbf{D})_{ia,ib}^{-1} = 0. \quad (45)$$

This last equation gives $N \times (q-1)^2$ equations that fix the unknown matrix \mathbf{D} , which is a functional of both \mathbf{f} and \mathbf{p} .

We can now compute the explicit Legendre transform of \mathcal{G} to obtain the cross-entropy, which is given by

$$\begin{aligned} \mathcal{S}[\mathbf{f}, \mathbf{p}] &= \mathcal{S}_{\text{IM}}[\mathbf{f}] - \frac{\varepsilon}{2} \text{Tr} \tilde{\mathbf{c}} \mathbf{J}^* - \frac{\varepsilon}{2} \text{Tr} \ln \mathbf{L} (\mathbf{L}^{-1} - \mathbf{J}^*) \\ &= \mathcal{S}_{\text{IM}}[\mathbf{f}] + \frac{\varepsilon}{2} \text{Tr} \left(\tilde{\mathbf{c}} (\mathbf{L} + \mathbf{D} + \tilde{\mathbf{c}})^{-1} \right) \\ &\quad + \frac{\varepsilon}{2} \text{Tr} \ln (\mathbf{L}^{-1} (\mathbf{L} + \mathbf{D} + \tilde{\mathbf{c}})). \end{aligned} \quad (46)$$

After setting $\varepsilon = 1$, Eqs. (44-46) coincide with the Eqs. (2), (3) and (5) of the main text since by definition we have $\mathbf{c} = \mathbf{L} + \tilde{\mathbf{c}}$.

The equation for the fields is in principle obtained by differentiation of the entropy with respect to the frequencies, as in Eq. (12). However we can take a shortcut by using properties of the Legendre transform, and noticing that

$$\begin{aligned} \frac{\delta \mathcal{S}[\mathbf{f}, \mathbf{p}]}{\delta f_\alpha} &= \sum_{\beta\gamma} \frac{\delta J_{\beta\gamma}^*}{\delta f_\alpha} \left(-p_{\beta\gamma} + \frac{\delta \mathcal{G}[\mathbf{f}, \mathbf{J}]}{\delta J_{\beta\gamma}} \right) + \left. \frac{\delta \mathcal{G}[\mathbf{f}, \mathbf{J}]}{\delta f_\alpha} \right|_{\mathbf{J}^*} \\ &= \left. \frac{\delta \mathcal{G}[\mathbf{f}, \mathbf{J}]}{\delta f_\alpha} \right|_{\mathbf{J}^*} \end{aligned} \quad (47)$$

This is important for our work because it means that we can find the equation for the fields before having to find the matrix \mathbf{D} , for which we don't have an explicit formula. The first order result is

$$\begin{aligned} h_{ia}^* &= \ln \left(\frac{f_{ia}}{f_{iq}} \right) + \sum_{j \neq i, b} (\mathbf{L} + \mathbf{D} + \tilde{\mathbf{c}})_{ia, jb}^{-1} f_{jb} \\ &\quad + \frac{1}{2} \sum_{i, bc} \gamma_{i; abc}^{(3)} D_{ib, ic} . \end{aligned} \quad (48)$$

This gives Eq.(4) of the main text, along with the well-known value of the fields inferred by the independent model, \mathbf{h}^{IM} .

Results for the Ising model

We now recast the relevant results of our expansion in the case of the Ising model, defined by its partition function

$$Z[\mathbf{h}, \mathbf{J}] = \sum_{\boldsymbol{\sigma}} \exp \left(\sum_i h_i \sigma_i + \sum_{i < j} J_{ij} \sigma_i \sigma_j \right) , \quad (49)$$

where here $\sigma = \pm 1$. We note the magnetizations $\langle \sigma_i \rangle = f_i$. The independent model Gibbs potential reads

$$\mathcal{S}_{\text{IM}}(\mathbf{f}) = - \sum_i \frac{1-f_i}{2} \ln \left(\frac{1-f_i}{2} \right) - \frac{1+f_i}{2} \ln \left(\frac{1+f_i}{2} \right) , \quad (50)$$

and the second derivative of this functional with respect to magnetizations is

$$L_{ij}^{-1} = - \frac{\delta^2 \mathcal{S}_{\text{IM}}}{\delta f_i \delta f_j} = \frac{1}{1-f_i^2} \delta_{ij} . \quad (51)$$

We will also use the notation $L_i = (1-f_i^2)$ for the diagonal elements of the matrix \mathbf{L} , without risk of confusions.

The order ε^2 in our expansion of \mathcal{G} for the Ising model reads

$$\begin{aligned} \mathcal{G}_2 &= \frac{1}{12} \sum_{ij} \gamma^{(3)}(f_i) (G_{ij}^3 + 3L_{ij}G_{ij}^2) \gamma^{(3)}(f_j) \\ &\quad - \frac{1}{8} \sum_i \gamma^{(4)}(f_i) G_{ii}^2 , \end{aligned} \quad (52)$$

where the vertex functions are given by

$$\gamma^{(n)}(x) = - \frac{(n-2)!}{2} \left[\frac{1}{(1-x)^{n-1}} + \frac{(-1)^n}{(1+x)^{n-1}} \right] . \quad (53)$$

After simplification, one obtains the Gibbs potential at order ε^2 ,

$$\begin{aligned} \mathcal{G} &= \mathcal{S}_{\text{IM}} + \sum_{i < j} J_{ij} f_i f_j - \frac{\varepsilon}{2} \text{Tr} \ln(\mathbb{K} - \mathbf{L}\mathbf{J}) \\ &\quad + \frac{\varepsilon^2}{3} \sum_{ij} f_i L_i^{-2} G_{ij}^3 L_j^{-2} f_j \\ &\quad - \frac{\varepsilon^2}{4} \sum_i L_i^{-2} G_{ii}^2 + \mathcal{O}(\varepsilon^3) , \end{aligned} \quad (54)$$

The results for the couplings, the fields and the cross-entropy are the same than that of the Potts model, once \mathbf{L} and $\gamma^{(3)}$ are replaced by their Ising counterparts.

FIG. 5. Diagrammatic expression of the high-temperature expansion of the rescaled $\tilde{\mathbf{D}}$ matrix. Open circles represent the site i , the lines are Γ factors and filled circles mean summation over a site index.

High-temperature expansion of the RMF couplings

We would like to gain more intuition in the role of the \mathbf{D} matrix, in the simplest case $q = 2$, so that \mathbf{D} is a diagonal matrix $D_{ij} = \delta_{ij} D_{ii}$. Defining rescaled (off-diagonal) correlations Γ as:

$$\Gamma_{ij} = (1 - \delta_{ij}) \left(L^{-1/2} \mathbf{c} L^{-1/2} \right)_{ij} , \quad (55)$$

We find that \mathbf{D} can be diagrammatically expressed in a high-temperature expansion (equivalent to an expansion in powers of Γ here), and we will show here only the result for the Ising case, up to order 4 in the high temperature expansion. By expanding Eq. (3) in power of Γ , one readily obtains the diagrammatic expression of the rescaled $\tilde{\mathbf{D}}$ matrix defined by:

$$\tilde{D}_{ii} = \left(L^{-1/2} \mathbf{D} L^{-1/2} \right)_{ii} = (\Gamma^2)_{ii} - (\Gamma^3)_{ii} + \dots \quad (56)$$

The diagrammatic representation of this is shown in Fig. 5, and this shows that \mathbf{D} resums ‘rings’ of \mathbf{c} going from the site i through an arbitrary number of intermediary sites before going back to i .

more common error used in the literature reads:

$$\Delta_J^2 = \frac{\sum_{i<j} (J_{ij}^* - J_{ij})^2}{\sum_{i<j} J_{ij}^2}, \quad (65)$$

with similar definitions for the fields. As stated in the main text, the reason is that the RMF couplings tend to be smaller than the true ones, especially deep in the glassy phase, i.e. we typically find $\mathbf{J}^* \simeq \alpha \mathbf{J}$, with $\alpha < 1$ getting smaller as σ_J increases. Equivalently, we find $\mathbf{h}^* \simeq \alpha \mathbf{h}$, with α of order one on average. This in turns implies that for a given realization of \mathbf{J} , Δ_J is typically close to one for the RMF inference. On the other hand, for other inference approximations, assuming they converge (for the Bethe and TAP approximation) or that \mathbf{c}^M can be inverted (for NMF and the approximation of Sessak and Monasson (SM) [20]), one typically find that the inferred couplings are very large compare to the true one, especially when \mathbf{c}^M is close to singular. This leads to very high errors, when computed with Δ_J . Comparison between our method and others would thus be very unfair using Δ_J as a measure of error.

Furthermore, we have shown that RMF, even when the couplings are too small, still gives a faithful representation of the data, in the sense that the typical configurations drawn from the inferred probability distribution are also the typical configurations of the true model (see Fig. 3). It is thus more interesting to see if the inferred couplings are well correlated with the true ones. This is captured by the Pearson correlation, at the cost of not knowing how the magnitude of \mathbf{J} and \mathbf{J}^* are related. For completeness, we show Δ_J and Δ_h averaged over the disordered realizations for the RMF, NMF and SM approximations in Fig. 7, which shows that RMF out-performs the other two methods. Note that for $\sigma_J \gtrsim 0.4$, we re-

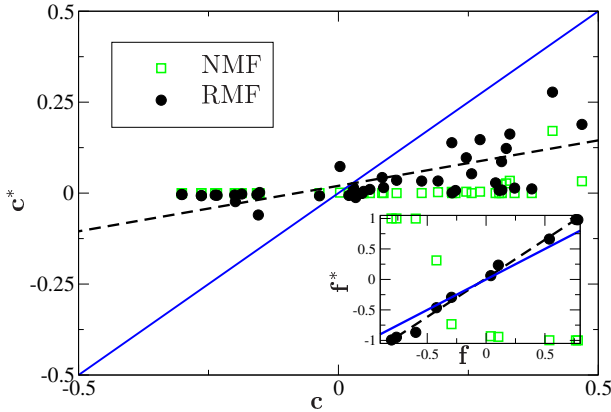


FIG. 8. Scatter plot of \mathbf{c}^* computed from RMF (black circles) or NMF (green squares) inference and \mathbf{c} computed from the original model, for one realization of the disorder (same as Fig. 1) for $\sigma_J = 0.7$. Full blue line is the line of slope 1. Black dashed line is the best linear regression for NMF, slope $\simeq 0.25$. Inset: scatter plot for the magnetizations. Slope of the black dashed line $\simeq 1.25$.

moved all cases where NMF and SM would not converge to meaningful results (being either infinite, or sometimes complex in the case of SM) in order to compute a meaningful error, whereas all RMF error are included, since it always converges.

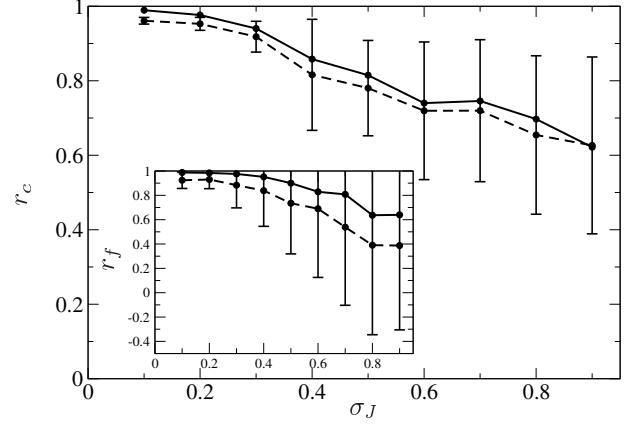


FIG. 9. Pearson correlations r_c between \mathbf{c} computed from RMF inference and \mathbf{c} computed from the original model, average over a hundred realizations of \mathbf{J} and \mathbf{h} . Full lines (resp. dashed lines) correspond to the inference made with $M = 10000$ configurations in the original dataset (resp. 100). The inset shows the average Pearson correlation for the frequencies r_f .

Frequencies and correlations from the inferred couplings

To judge whether the inferred couplings and fields from the RMF approximation are meaningful, we have drawn 1000 configurations via Monte-Carlo sampling, using the original couplings and fields ($\{\mathcal{C}\}$) and the RMF inferred ones ($\{\mathcal{C}_{\text{RMF}}\}$) (inference with $M = 100$). We have then obtained from these the corresponding frequencies \mathbf{f} and correlations \mathbf{c} (we will denote by $(\mathbf{f}^*, \mathbf{c}^*)$ those computed using the inferred couplings $(\mathbf{h}^*, \mathbf{J}^*)$). We show in Fig. 8 a scatter plot of the $(\mathbf{f}^*, \mathbf{c}^*)$ vs (\mathbf{f}, \mathbf{c}) for the same realization of the disorder than in Fig. 1, as well as the $(\mathbf{f}^*, \mathbf{c}^*)$ obtained using the NMF couplings. Because the NMF fields are really bad in the glassy phase, they strongly polarize the magnetization, and we clearly see that these are completely wrong for NMF. On the other hand, the RMF magnetization are really good. Concerning the correlations, we see that RMF gives relatively smaller correlation than the true one, which might be understood by the fact that the couplings tend to also be too small. On the other hand, NMF correlations are way too small (at least one order of magnitude too small). This is mostly due to the fact that the spins are strongly polarized, hence the orientation of a given spin is mostly independent from the others.

We have also computed the corresponding Pearson correlations between (\mathbf{f}, \mathbf{c}) obtained from $\{\mathcal{C}\}$, and (\mathbf{f}, \mathbf{c}) obtained from $\{\mathcal{C}_{\text{RMF}}\}$. The Pearson correlations averaged over the disorder realizations as a function of σ_J

are shown in Fig. 9. We see that the correlation is rather good even in the glass phase, and thus the RMF can be used to generate configurations that indeed reproduce the properties of the real data.